PHYSICAL REVIEW B VOLUME 54, NUMBER 4 15 JULY 1996-II

Theoretical and experimental study of positron annihilation with core electrons in solids

M. Alatalo, B. Barbiellini, M. Hakala, H. Kauppinen, T. Korhonen, M. J. Puska, K. Saarinen, P. Hautojärvi, and R. M. Nieminen
Laboratory of Physics, Helsinki University of Technology, FIN-02150 Espoo, Finland
(Received 27 October 1995)

A theory for calculating the momentum distribution of annihilating positron-electron pairs in solids is presented. To test the theory, momentum distributions are measured by the Doppler broadening of the annihilation radiation for several bulk metals and semiconductors, as well as for semiconductor alloys and for positrons trapped at vacancies in semiconductors. The theory is based on a two-particle description of the annihilating electron-positron pair. Then, the electron-positron correlation effects, i.e., the enhancement of the electron density at the positron, depend on the electronic state in question. The theory is suited for calculating the high-momentum part of the annihilation spectrum that arises from the core electrons and which can be measured by the Doppler broadening using coincidence techniques. The ideas of the theory are justified by a good agreement between theory and experiment in the case of positron annihilation in undefected bulk lattices. Moreover, the comparison of the theoretical and experimental spectra for alloys and vacancy defects tests the theoretical description for the positron distribution in delocalized and localized states, respectively. [S0163-1829(96)04327-5]

I. INTRODUCTION

Positron lifetime spectroscopy is a well established tool in studying the properties of vacancy-type defects in metals and semiconductors.[1,2] The fact that open volume defects can trap positrons makes it possible to distinguish between a defect-free sample and a sample containing vacancies. The average electron density at the vacancy is lower than in the bulk and therefore the lifetime of the trapped positron is increased compared to the value in the perfect bulk lattice. In the case of semiconductors, different charge states of the same vacancy can also be detected: ionic relaxations may change remarkably between adjacent charge states, and the larger the open volume of the defect the longer the positron lifetime.

The positron lifetime, however, is an integrated quantity, a single number that is not very sensitive to the chemical surroundings of the defect. On the other hand, the annihilation radiation contains much detailed electronic structure information to characterize the defect trapping the positron. This information can be extracted by the measurement of the Doppler broadening of the annihilation radiation.[3–5] As a result of the Doppler measurement, one obtains the one-dimensional momentum distribution of the annihilating electron-positron pairs. The low-momentum part of the spectrum arises mainly from the annihilation with valence electrons, whereas the high-momentum part is mainly due to the core electrons. The umklapp annihilations of the valence electrons decrease with increasing momentum and are therefore omitted in our calculations. The core electrons are tightly bound to the nuclei with specific binding energies and wave functions and therefore the high-momentum part of the electron-positron momentum distribution is characteristic for the chemical environment where the annihilation event took place. The simultaneous detection of the two 511 keV γ rays emitted from the same annihilation event leads to a significant reduction of the background.[4] The analysis of the momentum distribution curves up to rather large momenta becomes thus possible. The combination of the lifetime and the Doppler broadening measurement therefore provides a powerful tool for the identification of defects. In a recent paper,[5] we have demonstrated the applicability of the Doppler broadening method to the characterization of defects in compound semiconductors.

In this work, we emphasize that the measured high-momentum spectra are valuable data for testing the theoretical description of the positron states and annihilation characteristics in solids. In our previous paper,[5] we presented a simple computational scheme for the calculation of the high-momentum part of the Doppler spectra. The scheme was based on using the single-particle wave functions and local-density-dependent many-body corrections. This kind of approach has successfully been used to describe the momentum distribution of the annihilating *valence* electron-positron pairs.[6] The theoretical results for annihilations with *core* electrons were seen to be in good qualitative agreement with the experiment, especially when comparing the relative changes of quantities, such as the core annihilation (W) parameter, between the defect and the bulk positron states.[5] However, especially the absolute magnitudes of the momentum distributions differed significantly when comparing theory with experiment. One tractable reason for this discrepancy lies in the treatment of the electron-positron correlation, more specifically, in the enhancement of the electron density at a positron. In our previous work the many-body effects were included in an enhancement factor, calculated locally, using the *total* electron density at the positron site. This approach averages the electron-state dependence of the enhancement factor. The shortcomings of our previous calculations are puzzling because, on the other hand, the independent particle model (IPM) approach in which the correlations are omitted altogether (the enhancement factor $\gamma \equiv 1$) gives for bulk metals high-momentum spectra in quite a good agreement with experiment.[4]

In this paper, we present a more quantitative scheme for the calculation of the electron-positron momentum distribution using a state-dependent model for the enhancement. The idea behind the new scheme is that the two-particle description of the annihilating electron-positron pair appears more explicitly than in the scheme[5] used before. In practice, one determines the momentum distribution for each electron state using the IPM approximation and weights each curve by the corresponding annihilation rate. These annihilation rates in turn are calculated for all individual core states of the system studied, e.g., bulk or defected supercell, using the local-density approximation (LDA) (Ref. 7) or the generalized gradient approximation (GGA)[8] for the positron annihilation. These methods have been shown to give positron lifetimes in good agreement with experiment.[7–9] The GGA scheme has been shown to improve systematically the too short positron bulk lifetimes predicted by the LDA.[8] The comparison of the calculated high-momentum spectra with their experimental counterparts is a test for the core annihilation rates calculated within the LDA or the GGA. Moreover, a quantitative method for calculating the momentum distributions is desirable for the interpretation of near-surface Doppler spectra of thin material layers measured by slow positron beam techniques. For the samples of 1–5 μm in thickness the conventional lifetime spectroscopy cannot be used. The question of whether the sample contains defects able to trap positrons or not should be answered using the Doppler spectra. In this context, the quantitative comparison with theoretical predictions can strongly support the analysis.

In the case of a positron trapped by a defect, the theoretical description is more complicated than for a delocalized positron. Namely, the finite positron density may affect the electronic structure besides by causing the local enhancement at the positron also by changing the average electron density. The system can be treated by the two-component density-functional theory,[10] which solves the mutually self-consistent electron and positron densities. However, there exists different schemes[10–12] to treat the electron-positron correlations in the two-component theory and they can lead to quite different positron distributions. Moreover, there exists the so-called ''conventional'' method in which the electron density is calculated without the effect of the localized positron[2] and which therefore requires much less computational effort than a full two-component calculation. The positron lifetimes obtained within these different schemes are quite similar. In contrast, the magnitude of the core annihilation is very sensitive to the positron distribution. Therefore, the comparison of the theoretical high-momentum spectra with the experimental ones gives valuable information about the validity of the different schemes to describe localized positron states. In this work, we use only the conventional scheme and show that the results compare quite well with experiment. Further, we show that a large portion of the relevant information about the positron distribution is obtained directly from the total annihilation rates with core and valence electrons without the actual calculation of the momentum distribution. This enables an easy comparison of the results of different schemes with experiments.

The theoretical background of our approach is given in Sec. II, together with the practical considerations about the calculations. The experimental method is briefly described in Sec. III. In Sec. IV, we present results for the electron-positron momentum distributions in several bulk metals and semiconductors. The comparison with the experimental bulk results tests mainly the description of the electron enhancement at the positron. We present results also for semiconductor alloys and for defects in semiconductors along with the measured spectra. This allows us to draw conclusions about how faithful the theoretical description for the positron distribution is. Finally, our conclusions are presented in Sec. V.

II. THEORY

The Schrödinger equation for the two-particle system forming the annihilating pair with position vectors $\mathbf{r}_1$ and $\mathbf{r}_2$ is written as

$$\left(\sum_{i=1}^{2} h_i(\mathbf{r}_i)+V(\mathbf{r}_1,\mathbf{r}_2)\right)F(\mathbf{r}_1,\mathbf{r}_2)=EF(\mathbf{r}_1,\mathbf{r}_2), \tag{1}$$

where

$$h_i(\mathbf{r}_i)=\frac{\hbar}{2m}\nabla_i^2+V_i(\mathbf{r}_i) \tag{2}$$

is a one-particle Hamiltonian, $V_i(\mathbf{r})$ describes the effective potential seen by the particle i, and $V(\mathbf{r}_1,\mathbf{r}_2)$ is the pair interaction. We will adopt the Pluvinage method[13] to find an approximate solution of this equation. Let us write the two-particle wave function in the form $F(\mathbf{r}_1,\mathbf{r}_2)=G(\mathbf{r}_1,\mathbf{r}_2)f(\mathbf{r}_1,\mathbf{r}_2)$, where G and f are two unknown functions to be determined. The Schrödinger equation becomes

$$-\frac{\hbar}{2m}\left(\frac{\nabla_6^2 G}{G}+\frac{\nabla_6^2 f}{f}+2\frac{\nabla_6 G\cdot\nabla_6 f}{Gf}\right)+\sum_{i=1}^{2} V_i(\mathbf{r})+V(\mathbf{r}_1,\mathbf{r}_2) =E, \tag{3}$$

with the notation $\nabla_6=\nabla_1+\nabla_2$ and $\nabla_6^2=\nabla_1^2+\nabla_2^2$.

If one could find G and f, so that

$$\nabla_6 G\cdot\nabla_6 f=\epsilon Gf, \tag{4}$$

ϵ being a constant, the two-particle Schrödinger equation becomes separable:

$$\sum_{i=1}^{2} h_i(\mathbf{r}_i)G(\mathbf{r}_1,\mathbf{r}_2)=e_{\mathrm{orb}}G(\mathbf{r}_1,\mathbf{r}_2), \tag{5}$$

$$\frac{\hbar}{2m}\sum_{i=1}^{2}\frac{\nabla_i^2 f(\mathbf{r}_1,\mathbf{r}_2)}{f(\mathbf{r}_1,\mathbf{r}_2)}+V(\mathbf{r}_1,\mathbf{r}_2)=e_c, \tag{6}$$

$$E+\epsilon=e_{\mathrm{orb}}+e_c. \tag{7}$$

Above, $G(\mathbf{r}_1,\mathbf{r}_2)$ describes the orbital motion of the two particles ignoring each other, and $f(\mathbf{r}_1,\mathbf{r}_2)$ describes the correlated motion. For small $r_{12}=|\mathbf{r}_1-\mathbf{r}_2|$, we have the bare Coulomb attraction $V(\mathbf{r}_1,\mathbf{r}_2)=-1/r_{12}$ and for large r_{12}, the perfect screening gives $V(\mathbf{r}_1,\mathbf{r}_2)=0$.

In general, one cannot find such a G and an f so that ϵ is a constant. Therefore, our approximation consists of taking for ϵ an average value ϵ_a, such as

$$\epsilon_a = \frac{\langle F|\nabla_6 G\cdot\nabla_6 f\rangle}{\langle F|F\rangle} \tag{8}$$

and considering $\nabla_6 G\cdot\nabla_6 f-\epsilon_a F$ as a small perturbation.

The correlated motion is strongly dependent on the initial electron state j (without the presence of the positron). Obviously, the localized electron states near the nuclei are less affected by the positron than the s and p valence orbitals. We approximate the orbital motion by a product of single-particle orbitals as in the IPM, i.e.,

$$G_j(\mathbf{r}_1,\mathbf{r}_2)=\psi_+(\mathbf{r}_1)\psi_j(\mathbf{r}_2), \tag{9}$$

where ψ_+ is the positron wave function and ψ_j the electron wave function corresponding to the state j. Then, we assume that our potential $V(\mathbf{r}_1,\mathbf{r}_2)$ is a function of the distance r_{12} only, which is strictly true in the bulk for a very small and a very large r_{12}. Thus, we have solutions with the form $f_j(\mathbf{r}_1,\mathbf{r}_2)=u_j(r_{12})$. This is similar to the well known Jastrow approximation[14] for the pair wave function F. The adequacy of the Jastrow approximation can be tested by considering a model Hamiltonian of a positron-electron pair in a Coulomb field produced by a point charge $Z_{\rm eff}$. By using the variational Monte Carlo in the Jastrow approximation,[15] good agreement with a more accurate energy calculation employing Hylleraas-type wave functions[16] is obtained for $0.5<Z_{\rm eff}<1$.

The above formulation leads to a local annihilation rate for the state j,

$$\Lambda_j(\mathbf{r})=\pi r_e^2 c u_j^2(0)\psi_+^2(\mathbf{r})\psi_j^2(\mathbf{r}), \tag{10}$$

where r_e and c are the classical electron radius and the speed of the light, respectively. It is possible to define the constant term $u_j(0)$, such that the wave functions ψ_+ and ψ_j are normalized to unity and the total pair wave function is also properly normalized.

In principle, the knowledge of the two-particle potential allows the direct calculation of the wave function $u_j(r_{12})$. For the annihilation rate, only the contact value $u_j(0)$ is needed. Therefore we will adopt a different approach, which links $u_j(0)$ to the annihilation rate of the state j depending only on the electron and positron densities. This annihilation rate can be calculated using density functional schemes. By integrating the local annihilation rate of Eq. (10) over the $\mathbf{r}$ space, we find that

$$u_j^2(0)=\lambda_j/\lambda_j^{\rm IPM} \tag{11}$$

is the state-dependent enhancement. Above, $\lambda_j=\int d\mathbf{r}\,\Lambda_j(\mathbf{r})$ and $\lambda_j^{\rm IPM}=\pi r_e^2 c\int d\mathbf{r}\;\psi_+^2(\mathbf{r})\,\psi_j^2(\mathbf{r})$ are the actual annihilation rate for the state j and its approximation in the IPM, respectively. In order to obtain the state-dependent enhancement $u_j^2(0)$ we calculate λ_j in the LDA (Ref. 7) or in the GGA (Ref. 8) for positron annihilation, i.e.,

$$\lambda_j^{\rm LDA,GGA}=\pi r_e^2 c\int d\mathbf{r}\,\gamma^{\rm LDA,GGA}(\mathbf{r})\psi_+^2(\mathbf{r})\psi_j^2(\mathbf{r}), \tag{12}$$

where $\gamma(\mathbf{r})$ is a local enhancement factor depending in the LDA on the local electron density at point $\mathbf{r}$ and in the GGA also on the gradient of the electron density at that point. We use for $\gamma(\mathbf{r})$ the interpolation forms given in Ref. 8.

When the enhancement factor $u_j^2(0)$ is known, the momentum distribution for the electron-positron pair can be calculated as

$$\rho_j(\mathbf{p})=\pi r_e^2 c u_j^2(0)\left|\int d\mathbf{r}\exp(-i\mathbf{p}\cdot\mathbf{r})\psi_+(\mathbf{r})\psi_j(\mathbf{r})\right|^2. \tag{13}$$

This is the momentum distribution for the annihilation with the electron state j. The total electron-positron momentum distribution of the system is obtained by summing over different electron states. Equation (13) neglects the three-body correlations that do not contribute significantly at high momenta. However, this approximation can fail for the surfaces, because $V(\mathbf{r}_1,\mathbf{r}_2)$ is not screened outside the surface and consequently is not a function of the radius r_{12} only.

In the present scheme, the shape of the positron wave function is mainly determined by the repulsive interaction with the positive ion charge and the correlation effects are described by the Jastrow-like function. This picture could break down if the positron localizes within a distance that is smaller than the extent of the Jastrow function. Such a localization for the positron at defects in solids is unlikely. This is in accord with the conventional scheme,[2] in which the potential for a localized positron depends only on the electron density unperturbed by the presence of the positron.

An approximation frequently used for calculating the electron-positron momentum distribution consists of averaging the screening cloud over the electron states j,[17]

$$\rho_j(\mathbf{p})=\pi r_e^2 c\left|\int d\mathbf{r}\exp(-i\mathbf{p}\cdot\mathbf{r})\sqrt{\gamma(\mathbf{r})}\psi_+(\mathbf{r})\psi_j(\mathbf{r})\right|^2. \tag{14}$$

This approximation has been successfully used to describe the low-momentum region, in which annihilation with valence electrons dominates.[6] In our previous work,[5] we applied it also for the calculation of the core-electron part of the Doppler spectra. However, the position dependence of the enhancement factor causes in this approximation spurious effects at the high-momentum region, as will be shown below in the beginning of Sec. IV.

A model in which one constant enhancement factor is used for all core states has been succesfully used in describing the core-electron momentum distributions measured by angular correlation of annihilation radiation (ACAR) for Al or Cu.[18–20] On the other hand, a momentum-independent core enhancement factor has been found insufficient in describing the two-dimensional ACAR results for the alkaline metal Li.[21] This result may, however, be affected by the positron annihilation in the oxide layer of the sample.[22] The momentum dependence of the core enhancement factor has been discussed by Chiba *et al.*[23] and by Šob.[24] These works indicate that the core enhancement factor is momentum dependent, and the dependence is strong at the beginning of each metal series Na-Al, K-Zn, Rb-Cd. This reflects the low binding energies of the uppermost core levels and the corresponding high core polarizabilities. The momentum dependence of the core enhancement factor is then relatively weak at the end of each metal series (Al, Ni, Cu, Sn).

When restricting to a certain finite momentum region, our present approach can also be considered as using the same

TABLE I. Positron wave function parameters a and b for different elements. In the last column we show the outermost core states included in our calculations.

Material	Z	a	b	Outermost core state
Al	13	2.73	1.54	2p
Si	14	2.54	1.67	2p
P	15	2.27	1.81	2p
Ni	28	1.50	2.33	3p
Cu	29	1.53	2.28	3p
Ga	31	2.02	2.11	3d
Ge	32	2.09	2.16	3d
As	33	2.06	2.25	3d
In	49	2.05	2.73	4d
Sb	51	2.20	2.79	4d

constant enhancement factor for all core states. This is because the core annihilation for a given atom is dominated over a wide momentum region only by the outermost core orbital. However, when the momentum increases, the relative contributions of the deeper core states increase and become even dominating.[5] Thereby the state dependence of the enhancement factor reflects a certain degree of momentum-dependent enhancement.

In the present work, we calculate the core-electron wave functions needed in the above equations, using a density functional program for free atoms working in the LDA for the electron exchange and correlation. The positron potential is constructed as a sum of a Coulomb part and a correlation part obtained in the LDA or in the GGA.[8] For the positron wave function, we assume an isotropic form around each of the nuclei in the system. For practical purposes, the radial part of the positron wave function around a specific nucleus is approximated by the function

$$R_{10}^{+}(r) = C'[\mathrm{erf}(r/a)]^{b}, \tag{15}$$

where a and b are adjustable parameters and C' is a normalization parameter, which is not necessary to determine explicitly. We have used the linear-muffin-tin-orbital (LMTO) calculation within the atomic-spheres approximation (ASA)[25] to determine the self-consistent electronic structure and the ensuing positron wave function in the bulk systems. The parameters a and b have been found to be specific to the atom in question and rather transferable between different solid state systems such as different compounds or even to systems with point defects. A set of a and b parameters is given in Table I.

Figure 1 demonstrates the validity of the approximation of Eq. (15). It shows the positron wave function in the fcc Al calculated by the atomic-superposition method[26,27] in different directions with the Al nucleus in the origin. The wave function is very isotropic near the nucleus and is quite well described by the form of Eq. (15), the parameters of which are fitted to the spherically symmetric wave function obtained in the LMTO-ASA method. The parameters a and b obtained by fitting the wave functions around the Al nucleus in such compounds as AlP, AlAs, and AlSb are close to those obtained for the Al metal, and the shapes of the positron wave functions nearly coincide at distances shorter than

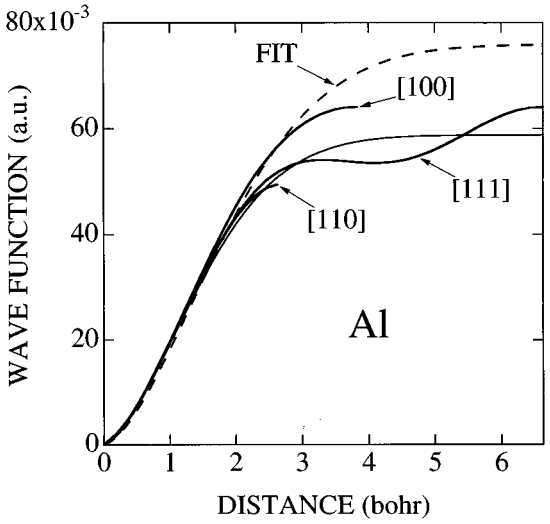

FIG. 1. Positron wave function in the fcc Al in different directions. The atomic-superposition method is used. The function of Eq. (15) fit to the positron wave function calculated with the LMTO-ASA method is shown as a dashed line. The wave functions are normalized to unity inside the conventional unit cell.

2 bohr from the nucleus. Because the electron wave functions of the core states approach zero already before 2 bohr in most cases of interest, the product of the electron and positron wave functions needed in calculations remains, discarding the normalization, nearly unchanged when moving the atom from one system to another. As a matter of fact, the small differences seen near the nucleus in Fig. 1 are mainly due to the fact that the positron potential arising from the self-consistent electron density is more repulsive than that calculated using the non-self-consistent atomic-superposition method.[9] The good agreement between the two calculation methods in Fig. 1 means that the fitting parameters could also be determined by using the atomic-superposition method.

The use of the free-atom core-electron wave function (quantum numbers n and l) and the isotropic positron wave function in Eq. (13) results in a spherically symmetric momentum distribution corresponding to the ion I of the system

$$\rho_{I,nl}(p) = 4\pi \frac{\lambda_{I,nl}}{\lambda_{I,nl}^{\mathrm{IPM}}} \pi r_e^2 c \left| \int_0^\infty dr\, r^2 R_{I,nl}^{-}(r) R_{I,10}^{+}(r) j_l(pr) \right|^2, \tag{16}$$

where $R_{I,nl}^{-}(r)$ is the radial part of the electron wave function and $j_l(pr)$ is the lth spherical Bessel function. $\lambda_{I,nl}$ and $\lambda_{I,nl}^{\mathrm{IPM}}$ are the partial annihilation rates calculated for the state nl of the atom I using a position-dependent enhancement [Eq. (12)] and within the IPM, respectively. Due to the use of the finite-range free-atom wave functions, the integration can be continued to infinity and oscillations, which result if the integration were abruptly cut, are avoided. The momentum distribution, which is compared with the experimental Doppler spectrum, is obtained by summing up the contributions of the core states n,l of all atoms I in the system and integrating over the high-momentum tail,

$$\rho(p_z)=\sum_{I,nl}\int_{p_z}^{\infty}dp\,p\rho_{I,nl}(p). \tag{17}$$

The division of the electron states to core and valence states is a subtle question. The criterion is that the core-electron wave functions are not affected when the solid is formed from free atoms. Then the free-atom wave functions can be used in calculating the momentum distributions. In principle, this approximation becomes valid at momenta high enough when deeper core states begin to dominate. This point may be at quite high momentum values if there are electron states in the system that are so delocalized that they cannot be described on the basis of atomic core orbitals but which, on the other hand, are relatively localized. The uppermost *d* band wave functions of transition or noble metals are examples of this kind of state. We will discuss the problem below in the case of Cu and GaAs. Our choices for the outermost electron states considered as core states are shown in Table I. These choices are usual also in the band-structure calculations, in which the valence electrons should be distinguished from the core electrons to be treated, for example, by the so-called frozen-core approximation. Naturally, all the inner states are included in the calculation of the momentum distribution, although the contribution of the innermost states at the relevant momentum regions is very small, due to the small annihilation rates.

The partial annihilation rates $\lambda_{I,nl}$ and $\lambda_{I,nl}^{\mathrm{IPM}}$ are calculated in this work using either the LMTO-ASA or the atomic-superposition method. In the case of defects and alloys with very large unit cells, only the latter has been used. In the atomic-superposition method, the electron density and the Coulomb potential are constructed non-self-consistently by overlapping free-atom densities and Coulomb potentials. The electron-positron correlation effects are included as a correlation potential and as an enhancement factor that are calculated using the superimposed electron density. The benefits of the atomic-superposition method are the use of the full three-dimensional geometry and its calculational speed, which especially for the defects in solids is orders of magnitude higher than that in self-consistent electronic structure calculations. As discussed below, the use of the non-self-consistent electron density instead of the self-consistent one may slightly change the annihilation rate with the core electrons.

The adaption of the atomic-superposition method for defects means that we use the conventional scheme for the localized positron states. The two-component density functional theory[10] is computationally very demanding and its application is also hampered by the poor knowledge of the electron-positron correlation effects in constructing the potential for the positron.[12] However, the two-component density functional theory with the electron-positron correlation formulated by Boroński and Nieminen[10] gives very similar positron distribution and annihilation characteristics as those obtained using the conventional scheme.[12] This gives justification for the use of the conventional scheme.

An important point in calculating the partial annihilation rates $\lambda_{I,nl}$ is the treatment of the enhancement part of the electron-positron correlation. The LDA gives positron lifetimes, which are consistently shorter than the experimental ones.[8] The GGA remedies quite successfully this discrepancy by reducing the annihilation in regions where the gradient of the electron density is large. Therefore, GGA reduces the annihilation rates of the core electrons. After demonstrating that the GGA scheme also gives momentum distributions in a better agreement with experiments than the LDA, we will adopt the GGA scheme for the rest of the calculations in this work.

III. EXPERIMENTAL METHOD

The experimental technique for the detection of the core-electron momentum distribution is the same as we have used earlier in Ref. 5. The 511 keV positron annihilation line is Doppler broadened by the amount $\Delta E=p_L c/2$, because of the longitudinal momentum component p_L of the annihilating positron-electron pair. Due to the momentum conservation, the relative direction of the two γ rays deviates from 180° by the small angle $\theta=p_T/m_0c$, where p_T is the transverse momentum component and m_0 is the electron mass. The equivalent momentum component $p_z=p_L=p_T$ can be related to either the Doppler shift or the angle θ by

$$p_z=2\Delta E/c=\theta m_0 c. \tag{18}$$

The Doppler broadening spectrum $f(\Delta E)$ can be measured by a high purity (HP) Ge detector and the momentum distribution $f(p_z)$ can thus be calculated from Eq. (18). By placing another γ detector in collinear geometry with the Ge detector, the two γ rays of $(511\pm\Delta E)$ keV can be simultaneously detected. This experimental procedure practically removes the background radiation from the Doppler spectrum and enables the detection of the positron-electron momentum distribution even up to $p=40\times10^{-3}m_0c$ (Ref. 5).

The Doppler spectrum in this work was measured by a HP Ge detector and a digitally stabilized multichannel analyzer (MCA) system. In order to detect the two 511 keV γ rays emitted from the same positron-electron annihilation event, a NaI scintillation detector was placed in collinear geometry with the Ge detector. When pulses from both detectors arrived, simultaneously the signal from the Ge detector was recorded in the memory of the multichannel analyzer. The pile-up rejection signal was used to gate the MCA and the remaining pile-up effect was minimized by using a 2 μs shaping time in the spectroscopy amplifier. With this setup the energy resolution, the full width at half maximum (FWHM) of the Ge detector at 511 keV, was only 1.6 keV $= 6.3\times10^{-3}m_0c$. The intensity of the remaining pile-up component was only about 2% of the core annihilation spectrum at $p_z=(10-40)\times10^{-3}m_0c$, and we subtracted it using numerical procedures. A constant background was also subtracted from all spectra.

The experiments were performed in bulk metals and semiconductors as well as in samples containing vacancy defects. The measurements in Al, Ni, and Cu were done in well annealed single crystals. The positron lifetime results in these samples (170, 107, and 120 ps, respectively) indicate that the samples are free of positron trapping at vacancy type defects. The Si sample was grown by the floating zone refinement method and its impurity concentration was very low (resistivity $>10^4\Omega$ cm). The Ge high-purity sample had an impurity concentration of less than $10^{12}\mathrm{cm}^{-3}$. The undoped GaAs, InP, and GaSb samples were liquid-encapsulated Czo-

chralski grown single crystals. The positron lifetime results on all bulk semiconductor samples (218 ps for Si, 228 ps for Ge, 231 ps for GaAs, 244 ps for InP, and 258 ps for GaSb) also indicate that these samples are free of vacancy defects acting as positron traps.

In order to investigate electron momentum distributions at vacancy defects, we studied electron irradiated InP. After annealing at 300 K, the vacancies present in semi-insulating Fe-doped InP give a positron lifetime of 283 ps, whereas a positron trap with a lifetime 267 ps is observed in *n*-type S-doped InP. These vacancies have been identified as the In vacancy (283 ps) and the P vacancy (267 ps), respectively.[5,28] However, the vacancy concentrations in the samples are not large enough to induce complete positron trapping, and the Doppler spectra have to be decomposed in order to obtain the annihilation lines of positrons trapped at vacancies. This can be achieved by combining positron lifetime and Doppler broadening experiments. Both the average lifetime τ_{av} and the positron-electron momentum distribution $f(p_z)$ are linear combinations of the bulk (subscript b) and vacancy (subscript v) responses:

$$\tau_{\mathrm{av}}=(1-\eta_v)\tau_b+\eta_v\tau_v\,, \tag{19}$$

$$f(p_z)=(1-\eta_v)f_b(p_z)+\eta_v f_v(p_z), \tag{20}$$

where η_v is the fraction of positron annihilations at the vacancy. Since the decomposition of the positron lifetime spectrum yields both τ_v and τ_{av}, the momentum distribution $f_v(p)$ can be solved from Eqs. (19) and (20) provided that the bulk distribution $f_b(p)$ is known. The decomposition procedure increases the statistical scattering of the data, and therefore the positron-electron momentum distribution for the vacancy is often not as accurate as that in the bulk.

The Doppler spectrum in all the samples mentioned above was measured by placing a ^{22}Na positron source between two identical sample pieces. The positron source was prepared by evaporating carrier-free ^{22}NaCl solution onto a 1 μm Al foil and the activity of the positron source was 17 μCi. A coincidence count rate of 170 s^{-1} was obtained when the Ge detector (efficiency 20%) was at a distance of 22 cm from the source and sample. The peak-to-background ratio in this setup was 2×10^4 and the total number of the collected annihilation events was $(2-4)\times10^7$.

In order to study alloying effects in the Doppler broadening spectrum, experiments were performed in 2.5 μm thick undoped $Al_{0.25}Ga_{0.75}As$ and undoped $Al_{0.36}Ga_{0.15}In_{0.49}P$ overlayers grown by the molecular beam epitaxy technique. These samples have been used earlier to study the *DX* centers. It was concluded that the undoped samples are free of vacancy defects acting as positron traps.[29–31] A low-energy positron beam with an incident positron energy of 15 keV was used for the Doppler broadening experiments of these layers. With this positron energy, the contributions from the annihilation events at the surface and in the substrate were negligible. A coincidence count rate of 80 s^{-1} was obtained in the positron beam experiments with a peak-to-background ratio of 2×10^4. The total number of the collected annihilation events was 2×10^7.

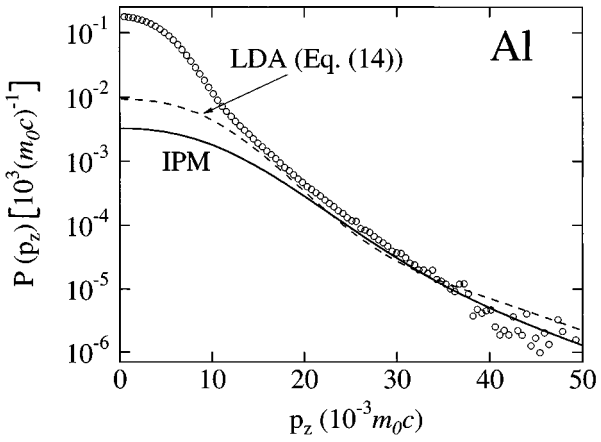

FIG. 2. Positron annihilation probability density $P(p_z)$ for bulk Al. The experimental data (circles) are shown together with two different theoretical approximations: IPM (solid line) and the old scheme based on Eq. (14) (dashed line).

IV. RESULTS AND DISCUSSION

In order to compare the experimental spectra and the theoretical momentum distributions calculated by different schemes they have to be properly normalized. The areas of the experimental spectra are scaled to unity, whereas the areas below the theoretical curves are equal to

$$\frac{\lambda_c}{\lambda_{\mathrm{tot}}}=\frac{\Sigma_{I,nl}^{\mathrm{core}}\lambda_{I,nl}}{\lambda_{\mathrm{tot}}}, \tag{21}$$

where λ_c is the annihilation rate with all the core electrons of the system and λ_{tot} is the total annihilation rate, i.e., the inverse of the positron lifetime. In the GGA and LDA schemes, the calculated λ_{tot} values are used but, in the IPM scheme, we have to use the experimental annihilation rate in a way that is similar to Ref. 4. The theoretical positron lifetimes used can be found in Ref. 8. With these normalizations, we obtain from the theoretical $(\rho(p_z))$ and experimental $(f(p_z))$ data the annihilation probability densities $(P(p_z))$ as a function of the momentum. In order to mimic the effects of the finite experimental resolution, the theoretical curves are convoluted before the comparison with a Gaussian function with a FWHM of $6.3\times10^{-3}m_0c$.

Before showing results obtained with our theoretical scheme, we will demonstrate the inadequacy of the old scheme based on Eq. (14). In Fig. 2, the theoretical core momentum distribution calculated using Eq. (14) for the Al metal is compared with the IPM result and the measured spectrum. In order to show the theoretical trends as clearly as possible, the convolution of the theoretical curves with the Gaussian is not performed in this figure. The effect of the enhancement in Eq. (14) is to raise especially the low-momentum part, because the enhancement increases with decreasing electron density and therefore it weights preferably the electron wave functions with the largest extent and the lowest momentum. It can be also seen that the curve calculated using Eq. (14) comes for certain momentum values close to and even crosses the IPM result. This kind of behavior means that there are oscillations in the momentum-dependent enhancement $\rho_j(p)/\rho_j^{\mathrm{IPM}}(p)$. These oscillations

have been reported already earlier.[6,32] At the highest momenta shown, the enhancement $\rho_j(p)/\rho_j^{\mathrm{IPM}}(p)$ is seen not to approach unity, which is the natural IPM limit expected to be valid for the most tightly bound core electrons contributing in this region.[4] The scheme of Eq. (14) is thus unable to reproduce even the shape of the high-momentum part of the experimental Doppler spectra. Moreover, these theoretical results are very sensitive to the approximation of the enhancement factor $\gamma(\mathbf{r})$ (different LDA and GGA enhancement forms). Thus, the state selectivity of the enhancement seems to be more important for the momentum distribution calculation than for the annihilation rate calculations for which the LDA and the GGA models give reasonable results. In the following sections, we will compare the momentum distributions calculated by our scheme with the measured ones.

A. Simple bulk metals and semiconductors

In this section, we will concentrate on bulk metals and semiconductors having a simple lattice with at most two types of different atoms, in contrast to alloys discussed below. The momentum distributions calculated for bulk Al and Si, using Eqs. (16) and (17) within the IPM, GGA, and LDA schemes, are compared with the experimental Doppler spectra in Fig. 3. The LMTO-ASA results for the partial annihilation rates λ_j have been used (solid lines). In Fig. 3, one can see that at high momenta the shapes of the theoretical curves agree well with the experimental behavior. This justifies the use of the model of Eq. (16) where the shape of the momentum distribution is determined from the radial dependencies of the electron and positron wave functions and from the *relative* values of the partial annihilation rates λ_j.

According to Fig. 3, the IPM approximation, which neglects the correlated motion of the electron-positron pair, leads to too low intensities in comparison with the experimental curves. In contrast, the LDA gives too much annihilation at high momenta. In the case of Al, the LDA enhancement factor is about 2.5 for the $2p$ core orbital, which is practically the only contributing orbital at high momenta. The overestimation of the core annihilation is in agreement with the result that the positron lifetimes calculated within the LDA are shorter than the measured ones.[8] Finally, the momentum distributions calculated within the GGA agree very well with the experimental spectra at high momenta. For the Al $2p$ orbital, the GGA reduces the enhancement factor to a value of about 1.7. It can be seen that the GGA also slightly improves the shape of the momentum distribution relative to the IPM result. This is because the enhancement for the highest core states contributing most strongly at the low momenta is larger than the enhancement for the deeper core states dominating at the high-momentum region. We have found that the GGA results are also, for the other bulk systems studied in good agreement with experiments and, therefore, in the following the theoretical momentum spectra, are calculated using only the GGA results.

The momentum distributions for Al and Si calculated using the partial annihilation rates obtained in the atomic-superposition method are shown in Fig. 3 as dashed curves. In the case of Al, the atomic-superposition result is slightly *above* the LMTO-ASA result, but the difference is, in practice, negligible and hardly visible in the figure. The difference reflects the fact that for the metal the self-consistent valence electron density is due to formation of metallic bonds that are more delocalized than the non-self-consistent superimposed density. The ions are then less screened and more repulsive for the positron, thus decreasing the core annihilation. In the case of Si, the atomic-superposition curve is clearly *below* that calculated using the LMTO-ASA annihilation rates, worsening the agreement between theory and experiment. The difference can be explained by the fact that in Si the valence electrons form covalent bonds between the ions. In comparison with the atomic-superposition method the electron density at the bonds leads to the transfer of the positron density from the open interstitial regions towards the ion core regions. This causes the increase of the core annihilation rate. In the calculations for the simple bulk systems below, we have used the annihilation rates obtained with the LMTO-ASA method.

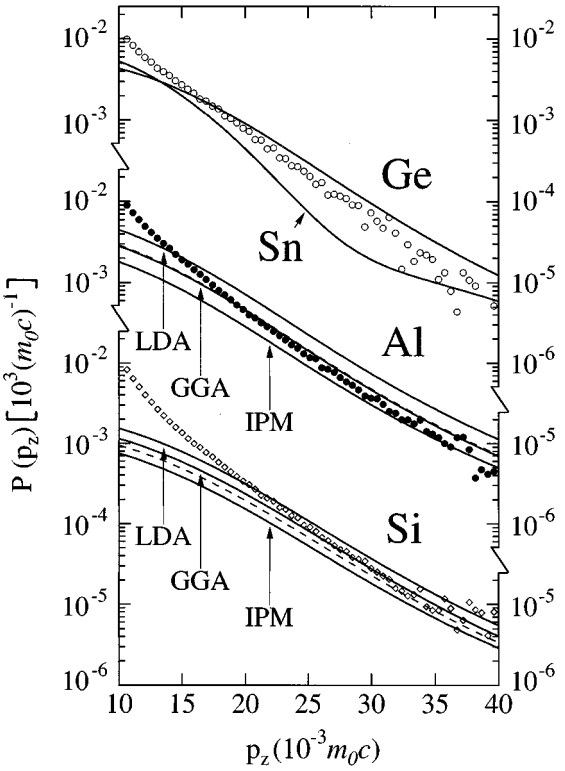

FIG. 3. Positron annihilation probability densities $P(p_z)$ for bulk Al, Si, Ge, and α-Sn. The experimental data (markers) are shown together with the different theoretical approximations (IPM, LDA, and GGA). For the α-Sn, there exists no measured data. The solid lines are obtained with the LMTO-ASA method. The dashed lines for Al and Si represent the GGA results calculated with the atomic-superposition method. In the case of Ge and α-Sn, only the GGA model and the LMTO-ASA method have been used. The theoretical curves are convoluted with a Gaussian in order to mimic the finite experimental resolution.

Before showing more examples of the high-momentum distributions, we want to give a better idea of the relative importance of the core annihilation in different materials and the differences between the GGA and LDA approaches for the enhancement. Therefore, Table II lists the core-electron contributions to the total annihilation rates in several cases.

TABLE II. Core-electron contribution relative to the total annihilation rate (λ_c) and the enhancement factor γ for the outermost core-electron states (see Table I) in perfect bulk crystals. The results are given both in the LDA and the GGA for positron annihilation.

Material	λ_c^{LDA} (%)		λ_c^{GGA} (%)		γ^{LDA}		γ^{GGA}	
	At. sup.	LMTO	At. sup.	LMTO	At. sup.	LMTO	At. sup.	LMTO
Al	9.4	9.3	6.0	5.8	2.48	2.53	1.68	1.71
Si	2.7	3.1	1.9	2.3	2.30	2.29	1.61	1.63
Ni	13.2	13.9	10.5	11.3	2.16	2.16	1.55	1.56
Cu	12.6	11.7	10.4	9.3	2.11	2.12	1.48	1.50
Ge	9.4	9.9	7.6	8.3	2.75	2.61	2.07	2.01
GaAs	11.1	11.7	9.1	10.2	3.05, 2.51	2.93,2.43	2.30, 1.89	2.32,1.87
InP	13.8	12.9	11.6	11.0	3.37, 2.13	3.02,2.12	2.53, 1.53	2.13,1.54
GaSb	11.4	10.7	9.5	9.5	3.12, 2.89	3.23,2.80	2.33, 2.18	2.56,2.13

For Al, the core annihilation is mainly due to the 2*p* orbital. The GGA reduces it by roughly one third. Also in the case of Si, 2*p* is the dominant core orbital, but the core contribution to the total annihilation rate is quite small, due to the large open lattice space. The effect of the GGA on the relative core contribution in Si is also small. For Ge and the III-V compound semiconductors shown in Table II, the dominant core orbital is the *d* orbital, which is highest in energy. The core contributions for these materials are relatively high, due to the spatial extent and high occupancy of the *d* orbitals. For these materials, the GGA reduces the core contribution slightly relative to the LDA values. The enhancement factors for the outermost core shells (see Table I) are also given in Table II. In the LDA, the enchancement factors are typically slightly above 2, but for the uppermost *d* electrons of the group III atoms they are around 3. The effect of the GGA is the reduction of the enhancement factor, nearly independently on the material, by 0.5–0.6.

Figure 3 demonstrates also how the characteristic features of the given core-electron wave functions are reflected in the Doppler spectra. Besides the different results for Al and Si discussed above, results for the perfect Ge and Sn crystals are shown. They are obtained by using the GGA scheme for the partial annihilation rates. For both Al and Si, the dominating core orbital is 2*p* and therefore the corresponding momentum distributions have quite similar shapes at high momenta. The magnitude is smaller for Si than for Al, because in Si the positron density concentrates strongly into the open interstitial region, decreasing the core annihilation rate. In Ge, the core annihilation mainly takes place with the 3*d* electrons. They are quite well localized in the **r** space and therefore the momentum distribution decays more slowly than in the case of Si. The higher intensity for Ge reflects the relatively large core annihilation rate (Table II). The most important core level for Sn (α-Sn with the diamond structure) is 4*d*. It has to be orthogonal against the 3*d*, which leads to a relatively large spatial extent and consequently to a localization in the momentum space. Indeed Fig. 3 shows that the curve for Sn decays much faster than that for Ge when the momentum increases. The characteristic behavior related to each core level can be used as a fingerprint when analyzing the chemical environment of the positron annihilating at a defect.[5] The experimental momentum distribution for Ge is also given in Fig. 3. It is seen to be in good agreement with the theoretical one, increasing the credence to the treatment of the enhancement effects in the new formalism.

Figure 3 shows the changes in the Doppler spectra seen when the elements belong to different *rows* of the Periodic Table. For comparison, we show in Fig. 4 how the change of the *column* will affect the qualitative features of the spectrum. We present both experimental and calculated spectra for the Cu and Ni that belong to adjacent columns of the Periodic Table. The positive charge of the nucleus is larger in the case of Cu, and therefore the core electrons are more tightly bound. This is reflected in a slightly smaller decay rate of the momentum distribution, in both the theoretical and experimental spectra, although the differences are very small. Moreover, the increased binding of the core electrons for Cu results in a smaller core annihilation rate and on average a smaller magnitude in the momentum distribution than those for Ni. It should be noted that the difference between the theoretical and experimental results up to the momentum around $35 \times 10^{-3} m_0 c$ is due to the 3*d* electrons, which, as discussed above, cannot be treated as core elec-

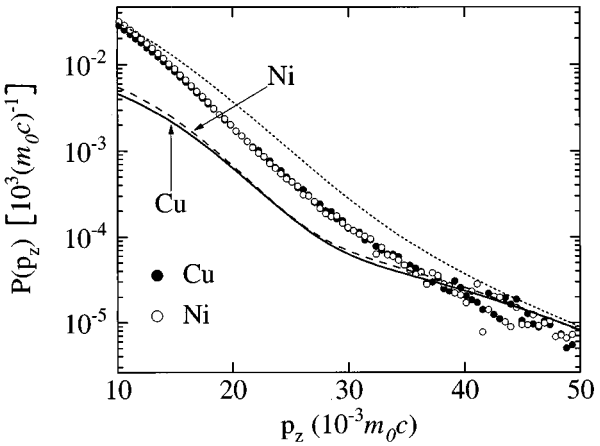

FIG. 4. Experimental and calculated positron annihilation probability densities $P(p_z)$ for bulk Ni (open circles, dashed line) and Cu (closed circles, full line). The theoretical curves are convoluted with a Gaussian in order to mimic the finite experimental resolution. The dashed line gives the probability density for Cu when the 3*d* electrons are included.

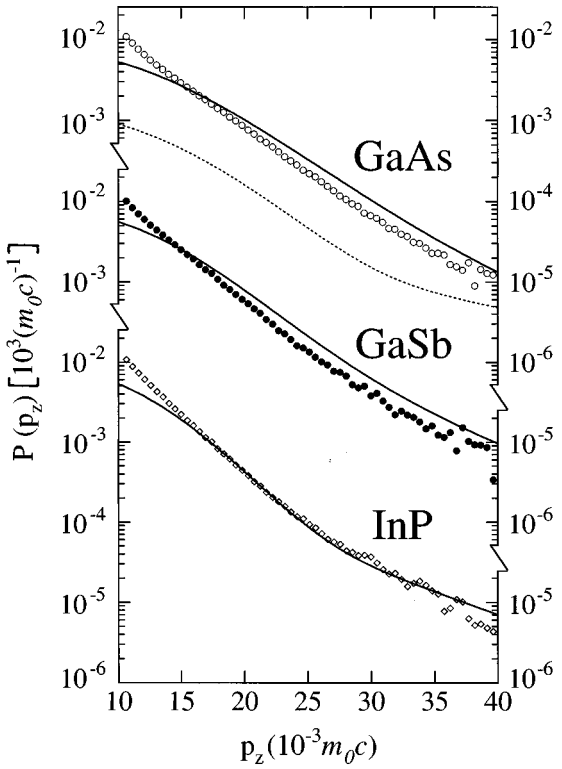

FIG. 5. Experimental (markers) and calculated (lines) positron annihilation probability densities $P(p_z)$ for GaAs, GaSb, and InP. The theoretical curves are convoluted with a Gaussian in order to mimic the finite experimental resolution. The dashed line gives the probability density for GaAs when the Ga and As 3*d* electrons are excluded.

trons in band-structure calculations. Figure 3 shows also the momentum distribution when the Cu 3*d* electrons are included as core electrons. In this calculation, the 3*d* partial annihilation rate is obtained by the atomic-superposition method. The intensity of the distribution is overestimated, although the decay rate agrees quite well with the experiment. It is also interesting to note that the theoretical results obtained without the 3*d* contributions show a difference between Ni and Cu, which is similar to the experimental result including also the annihilation with the 3*d* electrons.

The behavior of the Doppler spectra given in Fig. 5 for the bulk III-V compound semiconductors GaAs, GaSb, and InP can also be understood by discussing the characters of the most important core-electron levels contributing to the core annihilation. In all cases the uppermost *d* electrons cause the dominant contributions. In GaAs, all the *d* electrons belong to the $n = 3$ shell and therefore the momentum distribution decays relatively slowly. As shown in the figure, the omission of the Ga and As 3*d* electrons leads to an intensity clearly below the experimental values. Thus, in contrast to the case of Cu discussed above, it is important to include the 3*d* electrons in order to have a reasonable description for the high-momentum region. In GaSb half and in InP all of the *d* electrons belong to the $n = 4$ shell. As a consequence, the steepness of the curves increases when going from GaAs to GaSb and further to InP. The bending of the InP curve above the momentum of about $25\times10^{-3}m_0c$ is due to the fact that the contribution of the P 2*p* orbital overcomes that of the In 4*d* orbital.[5] The agreement between the theory and experiment is excellent in the case of InP. For GaAs and GaSb the shapes of the theoretical distributions are in good agreement with the experimental ones, but the theoretical curves are somewhat above the experimental spectra. This may reflect a slight overestimation of the partial annihilation rate with the Ga 3*d* orbitals or errors due to the use of the free-atom wave function instead of the actual one in the crystal. The true enhancement factor for the dominating Ga 3*d* orbitals may also have a momentum dependence omitted in our model.

B. Alloys

In order to demonstrate how the experiment-theory comparison can be used to test the theoretical positron distribution in more complex structures with several different types of atoms, we present results for the ternary alloy $Al_{0.25}Ga_{0.75}As$ and for the quatenary alloy $(Al_{0.7}Ga_{0.3})_{0.51}In_{0.49}P$. For the former, the theoretical results are based on the partial annihilation rates calculated using the LMTO-ASA method, whereas for the latter, the atomic-superposition method had to be used due to the large unit cell.

In Fig. 6(a), we present experimental and calculated Doppler spectra for bulk $Al_{0.25}Ga_{0.75}As$ compared with those for GaAs. According to both the theoretical and the experimental curves the introduction of Al atoms, which have no *d* electrons, reduces the magnitude of the Doppler spectrum. According to the theory, the reduction is slightly less than 20%. This is more than the Al atomic concentration of 12.5%, because of the relaxation of the positron density towards the open regions created around the smaller Al atoms. The interpretation is more difficult in Fig. 6(b), where we compare $(Al_{0.7}Ga_{0.3})_{0.51}In_{0.49}P$ with the pure InP. The curves are seen to cross each other twice, first around $20\times10^{-3}m_0c$ and again above $30\times10^{-3}m_0c$. This behavior can be explained as follows. At small momenta the curve for $(Al_{0.7}Ga_{0.3})_{0.51}In_{0.49}P$ has a smaller magnitude, since the contribution of In 4*d* is smaller than in InP. Above $20\times10^{-3}m_0c$, the contribution of In 4*d* is already significantly reduced, and Ga 3*d* becomes dominating. It gives a broader distribution than the In 4*d* and the curve for $(Al_{0.7}Ga_{0.3})_{0.51}In_{0.49}P$ rises above the InP curve. However, the In 4*d* contribution has a small but finite tail at very large momenta and this causes the curves to cross again at about $35\times10^{-3}m_0c$ where, in turn, the Ga 3*d* contribution has almost died out. This effect is more pronounced in the case of the calculated curves, which might suggest that the tail of In 4*d* is an artifact of the calculation. In this region, however, the scatter in the experimental data becomes too large for any strict comparison.

The good agreement between theory and experiment shows that the present method is able to handle correctly the spatial distribution of the positron wave function. The change in the chemical composition in one sublattice of a compound semiconductor alters the shape of the positron wave function which, in turn, causes changes to the Doppler spectrum. The fact that these changes can be reproduced in our calculations gives confidence to the theoretical scheme and to the GGA.

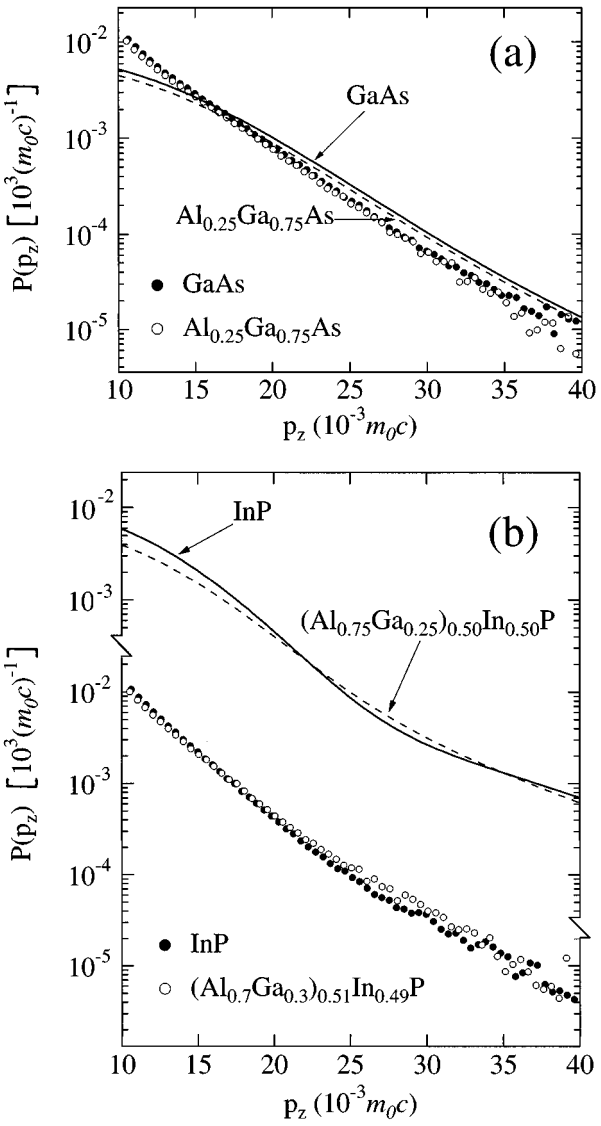

FIG. 6. (a) Experimental (markers) and calculated (lines) positron annihilation probability densities $P(p_z)$ for bulk $Al_{0.25}Ga_{0.75}As$ and GaAs. The solid (dashed) line represents the calculated GaAs ($Al_{0.25}Ga_{0.75}As$) and the closed (open) circles represent the experimental GaAs ($Al_{0.25}Ga_{0.75}As$). (b) Experimental and calculated positron annihilation probability densities $P(p_z)$ for bulk $(Al_{0.7}Ga_{0.3})_{0.51}In_{0.49}P$ and InP. The solid (dashed) line represents the calculated InP $[(Al_{0.75}Ga_{0.25})_{0.50}In_{0.50}P]$ and the closed (open) circles represent the experimental InP $[(Al_{0.7}Ga_{0.3})_{0.51}In_{0.49}P]$. The theoretical curves are convoluted with a Gaussian in order to mimic the finite experimental resolution.

C. Defects in semiconductors

The main use of the Doppler broadening technique of positron annihilation will be in the spectroscopy of defects in solids. In our previous paper,[5] we demonstrated how it can be used with the accompanied theoretical analysis in the defect identification. In this work, we show how the comparison of the theoretical and experimental Doppler spectra can be used to draw conclusions about the spatial distribution of the localized positron state. This is done in the context of some representative examples for defects in semiconductors, which have in recent years been subject of intensive studies by positron annihilation methods. However, first we have to consider some technical points.

Experimentally, the magnitude of the core annihilation rate is often monitored by the so-called W parameter of the Doppler spectrum, defined as

$$W=\frac{A_W}{A_{\mathrm{tot}}}, \tag{22}$$

where $A_{\mathrm{W}}=\int_{p_1}^{p_2}f(p_z)dp_z$ and $A_{\mathrm{tot}}=\int_0^{\infty}f(p_z)dp_z$, f being the measured spectrum. The momentum window p_1 - p_2 used in our experimental work, and therefore also used in our theoretical calculations, is the interval $(15–20)\times10^{-3}m_0c$. Within this window, the valence contribution has died out enough in the comparison with the core contribution and, on the other hand, the experimental background is not yet disturbingly large.[5]

In practice, the quantity used in the defect identification is the relative W parameter,

$$W_{\mathrm{rel}}=W_{\mathrm{defect}}/W_{\mathrm{bulk}}, \tag{23}$$

i.e., the ratio between the W parameters for the defect and perfect bulk systems. The relative W parameter allows a direct comparison between the defects in different materials. From the theoretical point of view, W_{rel} is a quantity that can be used to test the spatial distribution of the localized positron. This is because it is not very sensitive to the enhancement model (GGA or LDA) used. Moreover, the first approximation to it is given directly from the calculated core and total annihilation rates,

$$W_{\mathrm{rel}}\approx(\lambda_c/\lambda_{\mathrm{tot}})^{\mathrm{defect}}/(\lambda_c/\lambda_{\mathrm{tot}})^{\mathrm{bulk}}, \tag{24}$$

without the calculation of the momentum distribution. The approximate values agree in many cases within 1–2 % with the theoretical W_{rel} calculated using the momentum distribution and the optimal experimental window (see Table III). The agreement requires that the shapes of the momentum distributions for the bulk and the vacancy are rather similar. Then W_{rel} actually reflects the changes in the relative intensity of the core annihilation and it should remain practically constant, when another window at higher momentum is used. However, the approximative determination of W_{rel} may not be accurate enough, for example, when a vacancy-type defect is decorated by impurity atoms with a core-electron structure differing remarkably from the host atoms. An example of such a defect is the P vacancy–Zn complex, discussed in our previous work.[5]

We calculate the annihilation characteristics for the defects in semiconductors using the atomic-superposition method. A supercell geometry with periodic boundary conditions is used. The size of the supercell for the zinc-blende structures studied is 216 atomic sites. In the case of ideal vacancies, one site is left unoccupied and the neighboring ions are not allowed to relax from their ideal lattice positions. The moving of the ions in the atomic-superposition method is straightforward and the effects on positron annihilation characteristics can be studied. However, the method cannot, of course, determine from first principles the ground-state ionic positions. The differences in the electronic structure between the different charge states are not taken into

TABLE III. Theoretical and experimental positron lifetimes τ and W_{rel} parameters. The theoretical results are obtained with the atomic-superposition method using the GGA enhancement for ideal (unrelaxed) vacancies.

Material vacancy	τ^{GGA} (ps)	τ^{EXP} (ps)	$(\lambda_c/\lambda_{\mathrm{tot}})^{\mathrm{defect}}/(\lambda_c/\lambda_{\mathrm{tot}})^{\mathrm{bulk}}$	$W_{\mathrm{rel}}^{\mathrm{GGA}}$	$W_{\mathrm{rel}}^{\mathrm{EXP}}$
GaAs, bulk	232	231 [a]			
GaAs, V_{Ga}	265	260 [a]	0.75	0.77	0.74
InP, bulk	248	244 [b]			
InP, V_{In}	297	283 [b]	0.60	0.63	0.70 [b]
InP, V_{P}	262	267 [b]	1.03	1.02	0.94 [b]

[a]From Refs. 37 and 38.
[b]From Ref. 5.

account in the atomic-superposition method. However, it has been shown that the dependence of the positron lifetime on the charge state is quite small if the ionic relaxation is omitted.[33,34] Thus, the positron lifetime depends on the charge state mainly through the ionic relaxation. We can benefit from this fact when analyzing the experimental results. A relaxation pattern, which reproduces the experimental positron lifetime can first be searched for. Thereafter it can be checked if the calculated momentum distribution and/or the W_{rel} parameter agrees with the experiment, thereby supporting the defect identification.

In semiconductors, the positron probes only neutral or negatively charged defects.[2] For GaAs and InP, which are the materials of our examples, the atomic-superposition method within the GGA scheme reproduces well the experimental bulk lifetime values[8] (see Table III). The lifetimes calculated for the ideal cation vacancies are very close to the values extracted from experiments. As a matter of fact, in the experiments, the Fermi level is around the middle of the band gap and therefore the cation vacancies are in a negative charge state, presumably in the three state. According to the theoretical calculations,[12,35] the ions neighboring the ''clean'' negative cation vacancies tend to relax inwards towards the center of the vacancy. The good agreement obtained in the positron lifetime for the ideal cation vacancies means that the localized positron has a tendency of pushing the nearest neighbor atoms outwards close to their ideal vacancy positions. In the outward relaxation, the reduced repulsion between the positron and the ions compensates the elastic energy stored in the lattice. This picture is in accordance with recent two-component density functional calculations for the triply negative Ga vacancy (V_{Ga}^{-3}) in GaAs.[12]

The situation for the anion vacancies is more complicated, because they can exist in different charge states depending on the experimental conditions and the ionic relaxation may change drastically when the charge state changes.[11,35] Moreover, the relaxation patterns are complicated due to the symmetry-breaking Jahn-Teller relaxation. However, in the case of a singly negative P vacancy (V_{P}^{-}) in InP, the measured positron lifetime is, according to Table III, close to that calculated for the ideal vacancy.

Figure 7 shows the comparison between the momentum distributions for the In and P vacancies in InP. The theoretical curves are in a reasonable quantitative agreement with experiment, whereas in our previous work,[5] employing the theory based on Eq. (14) only, a qualitative agreement was possible. As discussed previously,[5] the difference between the In- and P-vacancy spectra is due to the fact that in the V_{P} the positron annihilates with a large probability with the $4d$ core electrons of the neighboring In ions. For the positron trapped by the In vacancy V_{In}, the annihilation with the In $4d$ electrons still dominates the core annihilation, but its intensity is smaller due to the larger distance of the second-neighbor In ions from the center of the vacancy. This can be seen in Fig. 8, which shows that the positron wave function at V_{In} is, due to spilling into the open interstitial regions, relatively large still in the close vicinity of the second nearest neighbor In ions. The good agreement between the theoretical and experimental momentum distributions is strong evidence for the ability of the conventional scheme to describe correctly the spatial extent of the positron state. Especially in the case of V_{In} the agreement is not a trivial result, because it requires an accurate description of the overlap between the positron density and the In ions, which are the next nearest neighbors of the vacancy.

The experimental and theoretical relative W parameters are collected in Table III. The W_{rel} parameters calculated for the ideal cation vacancies reproduce fairly well the experimental values. In fact, relaxing V_{In} in InP inwards by $\sim$4% of the bulk bond length gives the lifetime of 280 ps and W_{rel} 0.71, which are very close to the experimental values. The inwards relaxation is also in agreement with recent

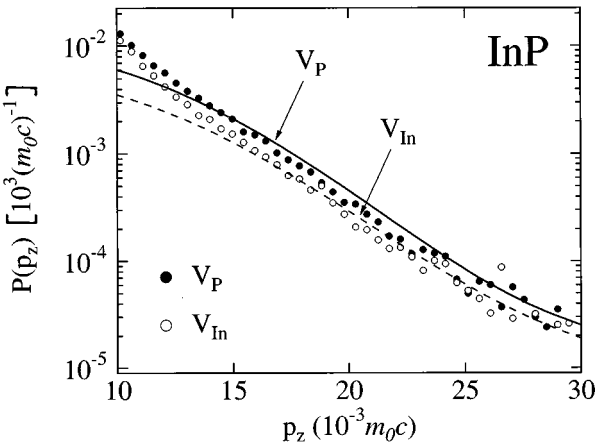

FIG. 7. Experimental (markers) and calculated (lines) positron annihilation probability densities $P(p_z)$ for the P vacancy (closed circles, full line) and the In vacancy (open circles, dashed line) in InP. The theoretical curves are convoluted with a Gaussian in order to mimic the finite experimental resolution.

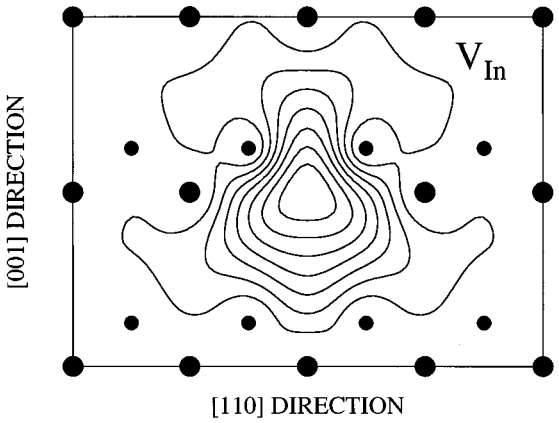

FIG. 8. The positron wave function at the In vacancy in InP. The figure shows a region of the (110) plane. The positions of In (P) ions are denoted by large (small) circles. The contour spacing is one- eighth of the maximum value.

first-principles calculations.[36] Moreover, similar relaxation has been found for V_{Ga}^{-3} in GaAs.[19] The theoretical W_{rel} parameter for the ideal P vacancy in InP is larger than unity. The relative core contribution to the total annihilation rate is larger for the ideal V_P than for the bulk, because of the large annihilation rate with the *d* electrons of the In atoms neighboring the vacancy. The experimental W_{rel} parameter for V_P is about 10% smaller than the theoretical one for the ideal vacancy. According to Table III, the experimental positron lifetime is somewhat longer than the theoretical positron lifetime. Both experiments therefore suggest a small outward relaxation for V_P. However, a simple breathing-type relaxation does not simultaneously bring the calculated W_{rel} parameter and the positron lifetime in such a good agreement with experiment as in the case of V_{In}.

In Ref. 12 the W_{rel} parameter was estimated for the triply negative Ga vacancy in GaAs using Eq. (24). The system was treated using the conventional scheme for the localized positron state and also applying two different schemes of the two-component density-functional theory. One of the two-component schemes is based on the construction by Boroński and Nieminen,[10] in which the electron-positron correlation energy at a given point depends both on the electron and positron densities at that point. In the other scheme proposed by Gilgien *et al.*,[11] the electron-positron correlation energy is taken from the limit where the positron density vanishes and thereby the correlation energy depends only on the electron density. All three schemes give similar positron lifetimes in reasonable agreement with experiment. The W_{rel} parameters for the ideal V_{Ga} estimated from the results of the conventional scheme and from those of the Boroński and Nieminen two-component theory are similar in magnitude, about 0.6–0.7. According to Table III, this value is in agreement with experiment. The scheme by Gilgien *et al.* gives for W_{rel} an estimate of about 0.35. The low value reflects a strong positron localization in the scheme by Gilgien *et al.* and is in clear disagreement with experiment.

V. CONCLUSION

Theoretical calculations for positron wave functions in solids have so far been used mainly for the estimation of the positron lifetimes and thereby for supporting the experimental defect identification. The positron lifetime is a parameter sensitive mainly to the open volume of a defect. The measurement of the core-electron part of the momentum distribution of the annihilating positron-electron pairs has been shown to give information on the chemical environment of the annihilation.[5] Therefore, a theoretical method combining the lifetime calculation and the reliable estimation of the core-electron contribution to the annihilation spectrum is needed for supporting the interpretation of the experimental results and the defect identification.

The comparisons of the calculated momentum distributions with the measured ones are crucial tests for the theories of positron states in solids. This is because the momentum distribution is much more sensitive to the positron distribution than the positron lifetime. This is true for the delocalized positron states, but especially in the case of localized positron states at defects, the comparison of the theoretical and experimental momentum spectra can be used to judge between different theoretical models.

In this work, we have developed an improved theory for the calculation of the core electron part of the momentum distribution of the positron annihilation radiation. Our theory is based on the two-particle picture of annihilating positron-electron pair. In practice, the momentum distribution for each electron state is calculated using the IPM approximation and adding up the individual contributions, weighted by the corresponding partial annihilation rates. The partial rates are calculated within the GGA for the positron annihilation. The good agreement between the calculated and experimental results for several bulk systems justifies the assumptions made in the theory. Especially, in the momentum region where the uppermost core electron states dominate the current method is found superior to the previous approaches.[4,5] In this region, the effects of the GGA in calculating the partial annihilation rates are the largest. This momentum region is also the most important one with respect to the identification of the chemical environment of the positron annihilation. The results for vacancies in semiconductors support the use of the conventional scheme for localized positron states. Moreover, they demonstrate the versality of the combined the positron lifetime and momentum distribution measurements with the accompanied theoretical calculations as an efficient tool for defect identification.

[1] For reviews see, P. Hautojärvi and C. Corbel, in *Positron Spectroscopy of Solids*, edited by A. Djasquier (IOS Press, Amsterdam, 1995), p. 491; M. J. Puska, Phys. Status Solidi A **102**, 11 (1987), and references therein.

[2] M. J. Puska and R. M. Nieminen, Rev. Mod. Phys. **66**, 841 (1994).

[3] *Positrons in Solids*, edited by P. Hautojärvi, Topics in Current Physics Vol. 12 (Springer-Verlag, Heidelberg, 1979).

[4] K. G. Lynn, J. R. MacDonald, R. A. Boie, L. C. Feldman, J. D. Gabbe, M. F. Robbins, E. Bonderup, and J. Golovchenko, Phys. Rev. Lett. **38**, 241 (1977); K. G. Lynn, J. E. Dickman, W. L. Brown, M. F. Robbins, and E. Bonderup, Phys. Rev. B **20**, 3566 (1979).

[5] M. Alatalo, H. Kauppinen, K. Saarinen, M. J. Puska, J. Mäkinen, P. Hautojärvi, and R. M. Nieminen, Phys. Rev. B **51**, 4176 (1995).

[6] M. Šob, in *Positron Annihilation*, edited by Yuan-Jin He, Bi-Song Cao, and Y.C. Jean, Mater. Sci. Forum, **175-178**, 855 (1995).

[7] K. O. Jensen, J. Phys. Condens. Matter **1**, 10 595 (1989).

[8] B. Barbiellini, M. J. Puska, T. Torsti, and R. M. Nieminen, Phys. Rev. B **51**, 7341 (1995); B. Barbiellini, M. J. Puska, T. Korhonen, A. Harju, T. Torsti, and R. M. Nieminen, Phys. Rev. B **53**, 16 201 (1996).

[9] M. J. Puska, J. Phys. Condens. Matter **3**, 3455 (1991).

[10] E. Boroński and R. M. Nieminen, Phys. Rev. B **34**, 3820 (1986).

[11] L. Gilgien, G. Galli, F. Gygi, and R. Car Phys. Rev. Lett. **72**, 3214 (1994).

[12] M. J. Puska, A. P. Seitsonen, R. M. Nieminen, Phys. Rev. B **52**, 10 947 (1995).

[13] P. Pluvinage, J. Phys. Radium **12**, 799 (1951); O. Dulieu and C. le Sech, Europhys. Lett. **3**, 975 (1987).

[14] R. Jastrow, Phys. Rev. **98**, 1479 (1955).

[15] A. Harju, S. Siljamäki, B. Barbiellini, and R. M. Nieminen (unpublished).

[16] O. V. Boev and K. P. Arefiev, Phys. Status Solidi B **106**, 481 (1981).

[17] S. Daniuk, G. Kontrym-Sznajd, J. Mayers, A. Rubaszek, H. Stachowiak, P. A. Walters, and R. N. West, in *Positron Annihilation*, edited by P. C. Jain, R. M. Singru, and K. P. Gopinathan (World-Scientific, Singapore, (1985), p. 43; S. Daniuk, G. Kontrym-Sznajd, A. Rubaszek, H. Stachowiak, P.A. Walters, and R. N. West, J. Phys. F **17**, 1365 (1987).

[18] J. Mader, S. Berko, H. Krakauer, and A. Bansil, Phys. Rev. Lett. 18 1232 (1976).

[19] R. P. Gupta and R. W. Siegel, Phys. Rev. B **22**, 4572 (1980).

[20] P. E. Mijnarends and R. M. Singru, Phys. Rev. B **19**, 6038 (1979).

[21] L. Oberli, A. A. Manuel, R. Sachot, P. Descout, and M. Peter, Phys. Rev. B **31**, 6104 (1985).

[22] L. Oberli, Ph.D. thesis, Geneva University, 1985 (unpublished).

[23] T. Chiba, G. B. Dürr, and W. Brandt, Phys. Status Solidi B **81**, 609 (1977).

[24] M. Šob, Solid State Commun. **53**, 255 (1985); in *Positron Annihilation*, edited by P. C. Jain, R. M. Singru, and K. P. Gopinathan (World Scientific, Singapore, 1985), p. 104.

[25] H. L. Skriver, *The LMTO Method* (Springer, New York, 1984). For the applications of the LMTO method to positron states, see A. K. Singh and T. Jarlborg, J. Phys. F **15**, 727 (1985), and Ref. 33.

[26] M. J. Puska and R. M. Nieminen, J. Phys. F **13**, 2695 (1983).

[27] A. P. Seitsonen, M. J. Puska, and R. M. Nieminen, Phys. Rev. B **51**, 14 057 (1995).

[28] M. Törnqvist, J. Nissilä, F. Kiessling, C. Corbel, K. Saarinen, A. P. Seitsonen, and P. Hautojärvi, Mater. Sci. Forum **143-147**, 347 (1994).

[29] J. Mäkinen, T. Laine, K. Saarinen, P. Hautojärvi, and C. Corbel, Phys. Rev. B **52**, 4870 (1995).

[30] J. Mäkinen T. Laine, J. Partanen, K. Saarinen, P. Hautojärvi, K. Tappura, T. Hakkarainen, H. Asonen, M. Pessa, J. P. Kauppinen, K. Vänttinen, M. A. Paalanen, and J. Likonen, Phys. Rev. B **53**, 7851 (1996).

[31] T. Laine, J. Mäkinen, K. Saarinen, P. Hautojärvi, C. Corbel, M. L. Fille, and P. Gibart, Phys. Rev. B **53**, 11 025 (1996).

[32] S. Daniuk, M. Šob, and A. Rubasek, Phys. Rev. B **43**, 2580 (1991).

[33] M. J. Puska, O. Jepsen, O. Gunnarson, and R. M. Nieminen, Phys. Rev. B **34**, 2695 (1986).

[34] M. Alatalo, M. J. Puska, and R. M. Nieminen, J. Phys. Condens. Matter **5**, L307 (1993).

[35] K. Laasonen, M. J. Puska, and R. M. Nieminen, Phys. Rev. B **45**, 4122 (1992).

[36] M. Alatalo, R. M. Nieminen, M. J. Puska, A. P. Seitsonen, and R. Virkkunen, Phys. Rev. B **47**, 6381 (1993); A. P. Seitsonen, R. Virkkunen, M. J. Puska, and R. M. Nieminen, *ibid.* **49**, 5253 (1994).

[37] C. Corbel, F. Pierre, P. Hautojärvi, K. Saarinen, and P. Moser, Phys. Rev. B **41**, 10 632 (1990).

[38] C. Corbel, F. Pierre, K. Saarinen, P. Hautojärvi, and P. Moser, Phys. Rev. B **45**, 3386 (1992).